Application of a Novel Iterative Denoising and Image Enhancement Technique in T1-Weighted Precontrast and Postcontrast Gradient Echo Imaging of the Abdomen

Improvement of Image Quality and Diagnostic Confidence

Sebastian Gassenmaier, MD, Saif Afat, MD,* Dominik Nickel, PhD,† Stephan Kannengiesser, PhD,† Judith Herrmann, MD,* Rüdiger Hoffmann, MD,* and Ahmed E. Othman, MD**

Objectives: The aim of this study was to investigate the impact of a novel iterative denoising and image enhancement technique in T1-weighted precontrast and postcontrast volume-interpolated breath-hold examination (VIBE) of the abdomen on image quality, noise levels, and diagnostic confidence without change of acquisition parameters.

Materials and Methods: Fifty patients were included in this retrospective, monocentric, institutional review board–approved study after clinically indicated magnetic resonance imaging of the abdomen including T1-weighted precontrast and postcontrast imaging. After acquisition of the standard VIBE ($VIBE_S$), images were processed with a novel reconstruction algorithm using the same raw data as for $VIBE_S$, resulting in a denoised and enhanced dataset ($VIBE_{DE}$). Two different radiologists evaluated both datasets in a randomized order regarding sharpness of organs as well as vessels, noise levels, artifacts, overall image quality, and diagnostic confidence using a Likert scale ranging from 1 to 4 with 4 being the best. Furthermore, in the presence of focal liver lesions, the largest lesion was measured in the postcontrast dataset, and lesion detectability was analyzed using a Likert scale (1–4).

Results: Precontrast and postcontrast sharpness of organs and sharpness of vessels were rated significantly superior by both readers in $VIBE_{DE}$ with a median of 4 (interquartile range, 0) compared with $VIBE_S$ with a median of 3 (1) (all P's < 0.0001). Precontrast and postcontrast noise levels were also rated superior by both readers in $VIBE_{DE}$ with a median of 4 (0) compared with $VIBE_S$ with a median of 3 (1) for precontrast and a median of 3 (0) (median of 3 [1] for reader 2) for postcontrast imaging (all P's < 0.0001).

Overall image quality was also rated higher with a median of 4 (0) in $VIBE_{DE}$ versus 3 (1) in $VIBE_S$ ($P < 0.0001$). Twenty-seven imaging studies contained liver lesions. There was no difference regarding the number and localization between the readers and between $VIBE_S$ and $VIBE_{DE}$. Lesion detectability was rated by both readers significantly better in $VIBE_{DE}$ with a median of 4 (0) compared with a median of 4 (1) for reader 1 and a median of 3 (1) for reader 2 ($P = 0.001$ for reader 1; $P < 0.001$ for reader 2). Consequently, diagnostic confidence was also significantly superior in $VIBE_{DE}$ versus $VIBE_S$ with a median of 4 (0) for both ($P = 0.001$). Interreader agreement resulted in a Cohen κ of 0.76 for precontrast analysis as well as of 0.76 for postcontrast analysis.

Conclusions: Application of a novel iterative denoising and image enhancement technique in T1-weighted VIBE precontrast and postcontrast imaging of the abdomen is feasible, providing superior image quality, noise levels, and diagnostic confidence.

Received for publication September 28, 2020; and accepted for publication, after revision, October 18, 2020.

From the *Department of Diagnostic and Interventional Radiology, Eberhard-Karls-University Tuebingen, Tuebingen; and †MR Applications Predevelopment, Siemens Healthcare GmbH, Erlangen, Germany.

Conflicts of interest and sources of funding: none declared.

Correspondence to: Ahmed E. Othman, MD, Department of Diagnostic and Interventional Radiology, Eberhard-Karls-University Tuebingen, Hoppe-Seyler-Straße 3, 72076 Tuebingen, Germany. E-mail: ahmed.e.othman@googlemail.com.

ISSN: 0020-9996/21/5605–0328
DOI: 10.1097/RLI.0000000000000746

Key Words: magnetic resonance imaging, noise, signal-to-noise ratio, abdomen

(*Invest Radiol* 2021;56: 328–334)

Magnetic resonance imaging (MRI) of the abdominal organs has become an integral part of clinical imaging during the last 2 to 3 decades.[1–3] One of the main foci of MRI consists of further characterization and examination of the organs of the abdomen.[4–7] However, abdominal MRI is a challenging task due to motion of the abdominal organs, especially caused by breathing.[8] Although traditional spin-echo sequences provide highly qualitative and robust images, this technique is too time-consuming for abdominal MRI due to motion.[9] Gradient echo (GRE) imaging presents an alternative with reduced imaging time due to shortened repetition time (TR).[10–12] Disadvantages of this technique are primarily increased sensitivity to magnetic field inhomogeneity and susceptibility artifacts.[13,14] Despite these issues, a contrast-enhanced T1-weighted 3-dimensional GRE imaging sequence has become widely established in abdominal MRI, known as volume-interpolated breath-hold examination (VIBE), liver acquisition with volume acceleration, T1-weighted high resolution isotropic volume examination, T1-weighted gradient echo, or 3D QUICK depending on the vendor.[15–17] However, the correct and proper execution of multiple breath-holds can be difficult in patients with impaired lung capacity, in elderly, or in pediatric patients. There are several methods available to overcome this problem. One possible approach uses respiratory gating. However, this technique can lead to overall long examination time, especially if breathing is not regular.[16] Another approach consists of free-breathing acquisitions, but these are not yet sufficiently clinically validated and established.[16,18,19] Probably the most common and widely established approach uses parallel imaging that allows reduction of breath-hold time.[20,21] A significant disadvantage of parallel imaging is loss of signal-to-noise ratio (SNR) proportional to the square root of the parallel imaging factor, which may impair diagnostic quality and readers' confidence, especially in the precontrast dataset.[20] There are several possibilities available for increase of SNR, for example, reduction of bandwidth, increase of TR, or increase of slice thickness. However, these approaches decrease diagnostic accuracy and increase acquisition time (TA), respectively.

Finally, both image resolution and SNR can be improved postacquisition using advanced image reconstruction techniques. A promising approach for SNR improvement in 3D GRE imaging is iterative denoising, which uses quantitative noise information and has been successfully applied to postcontrast acquisitions with native high resolution.[22,23]

Therefore, the aim of this study was to evaluate the impact of a novel iterative denoising and image enhancement technique in noncontrast and contrast-enhanced GRE MRI of the abdomen without change of acquisition parameters on image quality, noise levels, diagnostic confidence, and lesion detectability.

MATERIALS AND METHODS

Study Design

This retrospective, monocentric study was approved by the local institutional review board with waiver of informed consent. All study

procedures were conducted in accordance with the ethical standards as laid down in the 1964 Declaration of Helsinki and its latest revision in 2013.

Fifty patients who underwent a contrast-enhanced MRI of the abdomen between May and August 2020 were included in this study. Patients were identified using the institutional radiology information system.

MRI Acquisition Parameters

All imaging studies were conducted on 1.5-T MRI scanners (Siemens MAGNETOM Avanto fit and Aera; Siemens Healthcare, Erlangen; Germany) with patients in supine position using an 18-channel body coil and 32-channel spine coil setup. All patients received a bolus of contrast media adapted to their body weight (0.1 mmol/kg gadobutrol, Gadovist; Bayer Healthcare, Leverkusen, Germany) with a flow rate of 1.5 mL/s followed by a saline flush of 20 mL. An axial T1-weighted VIBE sequence was acquired precontrast and postcontrast (3 minutes postinjection) using the following parameters: voxel size of 1.2 × 1.2 × 3.0 mm, slice thickness of 3 mm, number of slices of 80, TR of 6.66 milliseconds, echo time (TE) of 2.39 milliseconds, flip angle of 10 degrees, matrix of 182 × 320, parallel imaging factor of 4, and TA of 16 seconds.

The same raw data that produced the standard reconstruction ($VIBE_S$) were then reconstructed again via a prototype implementation integrated into the scanner image reconstruction system, yielding a second image series ($VIBE_{DE}$).

Iterative Denoising Technique

A bank of thresholded orthogonal wavelet transforms was used for denoising of intermediate complex-valued, channel-combined images after parallel imaging reconstruction. As supplementary information, a quantitative map of the spatially varying noise level in the image domain was calculated with the help of the system's noise adjustment functionality and internal knowledge of noise-modifying operations, in particular including the "g-factor." This noise map allows spatial adaptation of the wavelet thresholds and iterative combination of denoised and original images for optimal noise removal according to Stein's Unbiased Risk Estimator.[24] After denoising, some edge enhancement (linear edge filter) was applied to compensate for any perceived loss in sharpness using the same strength as in the standard reconstructions. Reconstruction time per sequence was approximately 1 minute.

Image Evaluation

Image analysis was performed using a dedicated workstation (Centricity PACS RA1000; GE Healthcare, Milwaukee, WI). Images were independently evaluated by 2 radiologists with 5 years and 3 years of experience in body MRI. $VIBE_S$ and $VIBE_{DE}$ series were analyzed in a randomized order and blinded to clinical data as well as the original report. Image quality was qualitatively analyzed using a Likert scale ranging from 1 to 4 with 4 being the best. For image quality evaluation, the following criteria were assessed: sharpness of organ borders as well as sharpness of vessels (1, heavily blurred edges, organ borders and vessel walls not recognizable; 2, severely blurred edges, organ borders and vessel walls recognizable; 3, slightly blurred edges, organ borders and vessel walls recognizable; 4, no blurring with sharp organ borders and vessel walls), overall image quality (1, nondiagnostic; 2, poor image quality; 3, good image quality; 4, excellent image quality), and diagnostic confidence (1, no diagnosis possible; 2, severely reduced confidence, repetition of examination recommended; 3, good confidence; 4, very good confidence). Furthermore, the presence and extent of image artifacts as well as noise were assessed on a Likert scale ranging from 1 to 4 (1, excessive artifacts/noise; 2, severely hampered image quality by artifacts/noise; 3, slightly hampered image quality by artifacts/noise; 4, no visible artifacts/noise). In the presence of liver lesions, the number and localization of liver lesions was noted for up to 5 lesions per patient. Furthermore, the maximum axial diameter of the largest lesion was measured in the postcontrast dataset, and lesion detectability was evaluated (1, lesion border not detectable; 2, poor detectability of lesion border; 3, good detectability of lesion border; 4, excellent detectability of lesion border). As only T1-weighted precontrast and postcontrast sequences were available for reading under study conditions, no further characterization of liver lesions was performed.

Statistical Evaluation

Statistical software was used for analysis (SPSS Statistics Version 26; IBM, Armonk, NY). Parametric variables are displayed using mean ± standard deviation. Nonparametric variables are displayed using median and interquartile range in parentheses. The Wilcoxon signed-rank test was used for comparison of ordinal-scaled dependent data between the original and iteratively denoised image data sets. Bland-Altman analysis was performed to compare the size measurements of liver lesions between both readers. Linearly weighted Cohen κ was used to evaluate interreader agreement. P values below 0.05 were regarded as significant.

RESULTS

Patients' Characteristics

All examinations could be evaluated successfully. The mean patient age was 56 ± 18 years (range, 18–84 years). Most patients (n = 35) underwent abdominal MRI due to malignant tumors (mostly melanoma, n = 7; and hepatocellular carcinoma, n = 7). In 26 cases, there was no abnormal finding, whereas in 8 cases, metastatic disease was found. Further details are displayed in Table 1.

Interreader Variability

Interreader agreement was substantial for precontrast as well as postcontrast imaging (each Cohen κ of 0.76). Therefore, only the results of reader 1 are displayed in the following. The results of reader 2 are available in Tables 2 and 3.

TABLE 1. Patients' Characteristics

Characteristics	Values
Patients, n	50
Age, mean ± SD (range), y	56 ± 18 (18–84)
Indication for MRI examination, n	
Melanoma	7
Hepatocellular carcinoma	7
Neuroendocrine tumor	5
Breast cancer	4
Post-LTX	3
Other malignant carcinoma	12
Inflammatory disease	5
Other nonmalignant disease	7
Liver MRI findings, n	
Unremarkable	26
Metastatic disease	8
Hepatocellular carcinoma	4
Benign focal liver lesions	3
Liver cirrhosis	3
Other malignant findings	3
Other nonmalignant findings	3

LTX, liver transplantation; MRI, magnetic resonance imaging.

TABLE 2. Evaluation of Image Quality and Diagnostic Confidence in $VIBE_S$ and $VIBE_{DE}$

	Reader 1			Reader 2		
Characteristics	**$VIBE_S$**	**$VIBE_{DE}$**	***P***	**$VIBE_S$**	**$VIBE_{DE}$**	***P***
Sharpness organs precontrast	3 (1)	4 (0)	<0.0001	3 (1)	4 (0)	<0.0001
Sharpness organs postcontrast	3 (1)	4 (0)	<0.0001	3 (1)	4 (0)	<0.0001
Sharpness vessels precontrast	3 (1)	4 (0)	<0.0001	3 (1)	4 (0)	<0.0001
Sharpness vessels postcontrast	3 (1)	4 (0)	<0.0001	3 (0)	4 (0)	<0.0001
Noise precontrast	3 (1)	4 (0)	<0.0001	3 (1)	4 (0)	<0.0001
Noise postcontrast	3 (0)	4 (0)	<0.0001	3 (1)	4 (0)	<0.0001
Artifacts precontrast	4 (1)	4 (0)	0.025	4 (0)	4 (0)	0.083
Artifacts postcontrast	4 (0)	4 (0)	0.083	4 (0)	4 (0)	0.083
Overall image quality precontrast	3 (1)	4 (0)	<0.001	3 (1)	4 (0)	<0.001
Overall image quality postcontrast	3 (1)	4 (0)	<0.001	3 (1)	4 (0)	<0.001
Diagnostic confidence	4 (0)	4 (0)	0.001	4 (0)	4 (0)	0.001

VIBE, volume-interpolated breath-hold examination; $VIBE_S$, standard VIBE datasets; $VIBE_{DE}$, denoised datasets.

Qualitative Image Quality Evaluation of Precontrast Imaging

The sharpness of organ borders as well as vessels was evaluated significantly better in precontrast $VIBE_{DE}$ with a median of 4 (0) compared with precontrast $VIBE_S$ with a median of 3 (1) ($P < 0.001$). Precontrast $VIBE_{DE}$ was also rated with less noise than $VIBE_S$ with a median of 4 (0) versus 3 (1) ($P < 0.001$). There were only slightly more severe artifacts (motion and parallel imaging artifacts) found in $VIBE_S$ (median of 4 [1]) versus $VIBE_{DE}$ (median of 4 [0]; $P = 0.025$). Overall image quality of precontrast imaging was also rated significantly superior in $VIBE_{DE}$ with a median of 4 (0) versus a median of 3 (1) in $VIBE_S$ ($P < 0.001$). Figure 1 shows an example of precontrast imaging with additional SNR maps.

Qualitative Image Quality Evaluation of Postcontrast Imaging

Analogous to precontrast imaging analysis, postcontrast imaging was rated significantly better regarding sharpness of organ borders as well as vessels in $VIBE_{DE}$ compared with $VIBE_S$ (median of 4 [0] vs 3 [1]; $P < 0.001$). Noise levels were also rated to be significantly less in $VIBE_{DE}$ versus $VIBE_S$ with a median of 4 (0) compared with a median of 3 (0) ($P < 0.001$). There was no significant difference regarding artifacts (motion and parallel imaging artifacts) (both median of 4 [0], $P = 0.083$). Figure 2 demonstrates examples of occurred artifacts. Overall image quality was also evaluated to be higher in $VIBE_{DE}$ than in $VIBE_S$ with a median of 4 (0) versus 3 (1) ($P < 0.001$). Figure 3 shows an example of postcontrast imaging with additional SNR maps.

Diagnostic confidence levels were significantly superior in precontrast and postcontrast imaging in $VIBE_{DE}$ versus $VIBE_S$ with a median of 4 (0) for both datasets ($P = 0.001$). Figure 4 shows another imaging example of $VIBE_S$ and $VIBE_{DE}$.

Lesions Detection

Twenty-seven imaging studies with altogether 72 liver lesions were found. In 7 cases, multiple lesions (more than 5) were found. No difference was found between both readers or between standard and denoised datasets regarding the localization of lesions. The largest lesions were in 12 cases cystic lesions, in 9 cases metastatic lesions, in 3 cases hepatocellular carcinoma, and in 1 case focal nodular hyperplasia. There was no significant difference between lesion size between $VIBE_S$ (18 ± 11 mm) and $VIBE_{DE}$ (17 ± 11 mm) for reader 1 ($P = 0.743$). However, there was a slight significant difference between $VIBE_S$ (18 ± 12 mm) and $VIBE_{DE}$ (19 ± 12 mm) for reader 2 ($P = 0.010$). Intraclass correlation coefficient (ICC) was excellent between both readers (ICC > 0.9). Lesion detectability was rated by both readers significantly better in $VIBE_{DE}$ with a median of 4 (0) compared with a median of 4 (1) for reader 1 and a median of 3 (1) for reader 2 ($P = 0.001$ for reader 1; $P < 0.001$ for reader 2) (see Table 3 for further details). Figures 5A and B show Bland-Altman plots for readers 1 and 2.

DISCUSSION

This study investigated a novel iterative denoising and image enhancement approach for T1-weighted VIBE precontrast and postcontrast imaging of the abdomen. The results show that image quality, noise levels, sharpness of body structures, as well as diagnostic confidence can be significantly improved via this approach compared with the standard reconstruction.

T1-weighted VIBE imaging is a key element in current abdominal MRI.[17] Gradient echo imaging provides swift and precise imaging for basically all abdominal pathologies with minimized motion artifacts. Compared with traditional TSE or even SE techniques, the major disadvantages of GRE sequences are an increased risk for susceptibility artifacts due to magnetic field inhomogeneities.[10] Another drawback, especially important in abdominal MRI, is given by the necessity of breath-holds in conventional Cartesian VIBE sequences leading partially to compromised image quality, especially in patients of very young age or in elderly people. A possible solution for this issue was demonstrated by Chandarana et al[16] using a free-breathing radial 3D GRE (VIBE) sequence with comparable image quality to standard breath-hold VIBE. However, the major disadvantage of this technique lies in its longer TA. Another disadvantage of radial readout compared with Cartesian readout is based on reduced vessel-tissue contrast.[25]

TABLE 3. Lesion Detectability and Lesion Size in $VIBE_S$ and $VIBE_{DE}$

	$VIBE_S$			$VIBE_{DE}$		
Characteristics	**Reader 1**	**Reader 2**	**ICC/ κ**	**Reader 1**	**Reader 2**	**ICC/ κ**
Lesion size, mm	18 ± 11	18 ± 12	0.99	17 ± 11	19 ± 12	0.99
Lesion detectability	4 (1)	3 (1)	0.78	4 (0)	4 (0)	0.78

VIBE, volume-interpolated breath-hold examination; $VIBE_S$, standard VIBE datasets; $VIBE_{DE}$, denoised datasets.

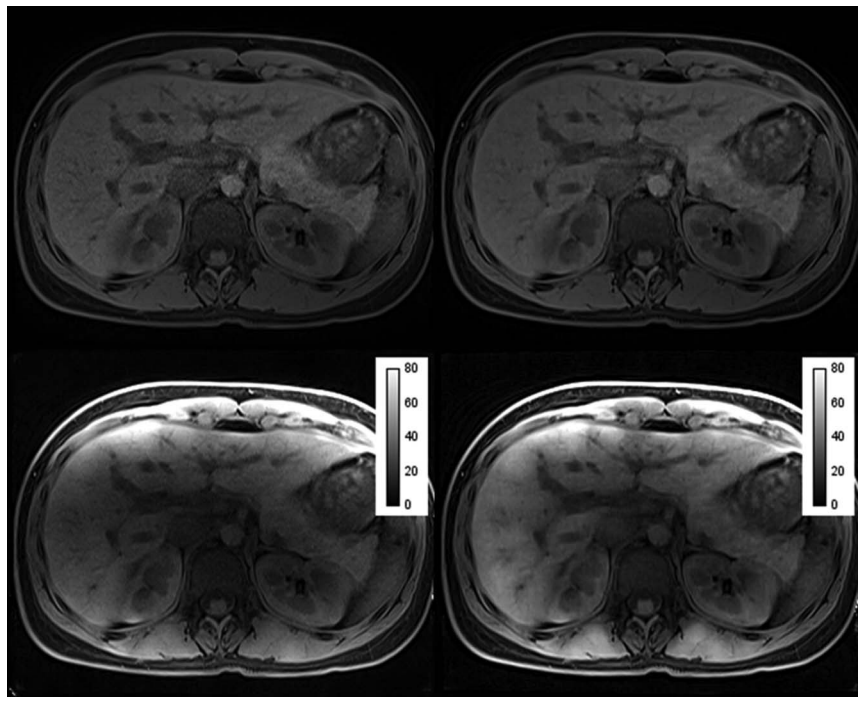

FIGURE 1. Image shows an example of a precontrast dataset with the reconstructed images in the upper row and signal-to-noise ratio (SNR) maps in the bottom row with an SNR scale bar (multiplicated by the factor of 10). The left column shows standard imaging ($VIBE_S$), whereas the right column shows the iteratively denoised dataset ($VIBE_{DE}$). The $VIBE_{DE}$ dataset shows lower noise levels and an increase of SNR with a more homogeneous distribution compared with the $VIBE_S$ dataset. This SNR improvement affects especially the central parts of the body (eg, major vessels as aorta, vena cava inferior, and portal vein). In addition, SNR levels throughout the liver parenchyma or more homogeneous with clearly improved SNR in the central liver segments as well as the peripheral parts of parenchyma.

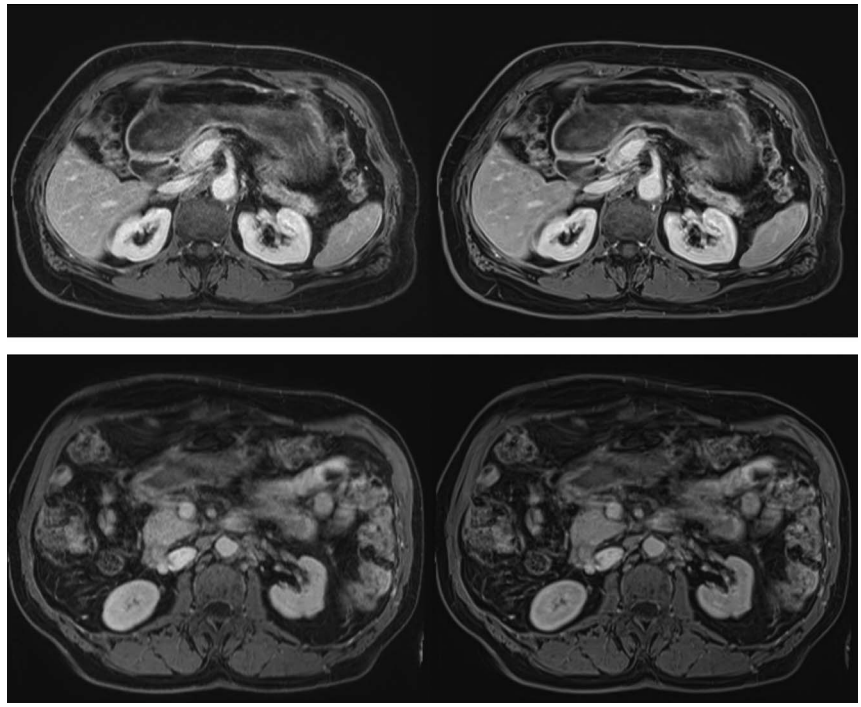

FIGURE 2. Image demonstrates common artifacts that occurred in our study cohort in postcontrast imaging with standard imaging reconstruction ($VIBE_S$) in the left column and iterative denoising ($VIBE_{DE}$) in the right column. The upper row shows an example of a parallel imaging artifact with a noise band affection of the delineation of the aorta and superior mesenteric artery. This effect was reduced in $VIBE_{DE}$. The bottom row shows an example of blurred edges of the intestine due to intestinal motion. Although in $VIBE_{DE}$ the edges of the intestine appear slightly sharper, effects of motion are still visible.

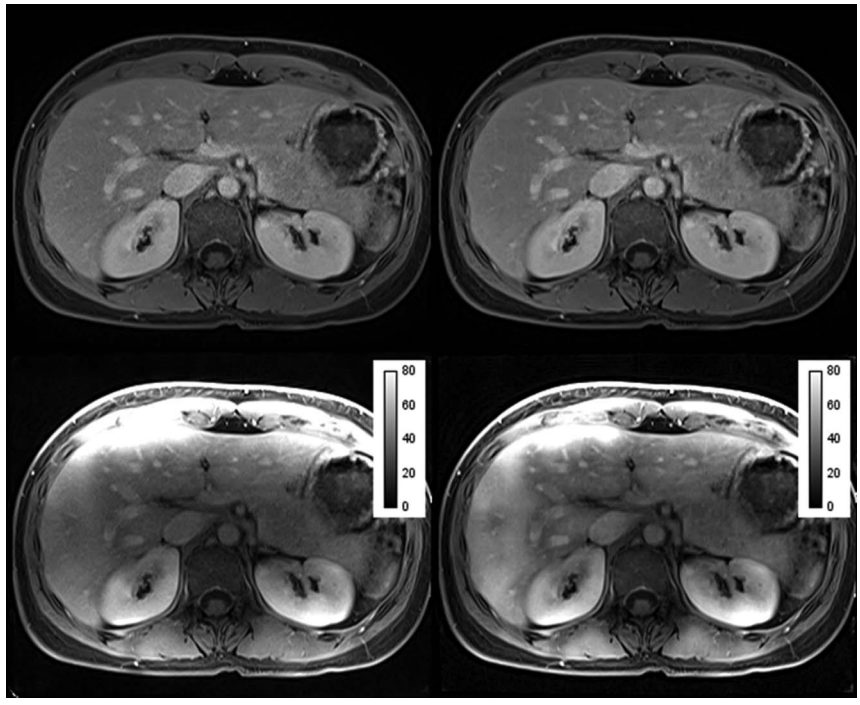

FIGURE 3. Image shows an example of a postcontrast dataset with the reconstructed images in the upper row and signal-to-noise ratio (SNR) maps with an SNR scale bar (multiplicated by 10) in the bottom row. The left column shows standard imaging ($VIBE_S$), whereas the right column shows the iteratively denoised dataset ($VIBE_{DE}$). Analogous to the precontrast dataset, noise levels as well as SNR were improved in the $VIBE_{DE}$ dataset with a more homogeneous distribution, especially affecting the peripheral parts of the liver parenchyma of the right liver lobe and the central body parts. Compared with precontrast imaging, the effect of SNR improvement is less pronounced.

Although some experimental applications of self-gated 4D liver MRI or combinations of parallel imaging, compressed sensing, and radial readout have been reported, these techniques are still not widely established in clinical routine.[25,26] One of the most common approaches to reduce acquisition and breath-hold time is parallel imaging. Unfortunately, high parallel imaging acceleration factors lead to a significant decrease in image quality and increase in noise as SNR is decreased by the square root of the acceleration factor. This issue impedes the usage of

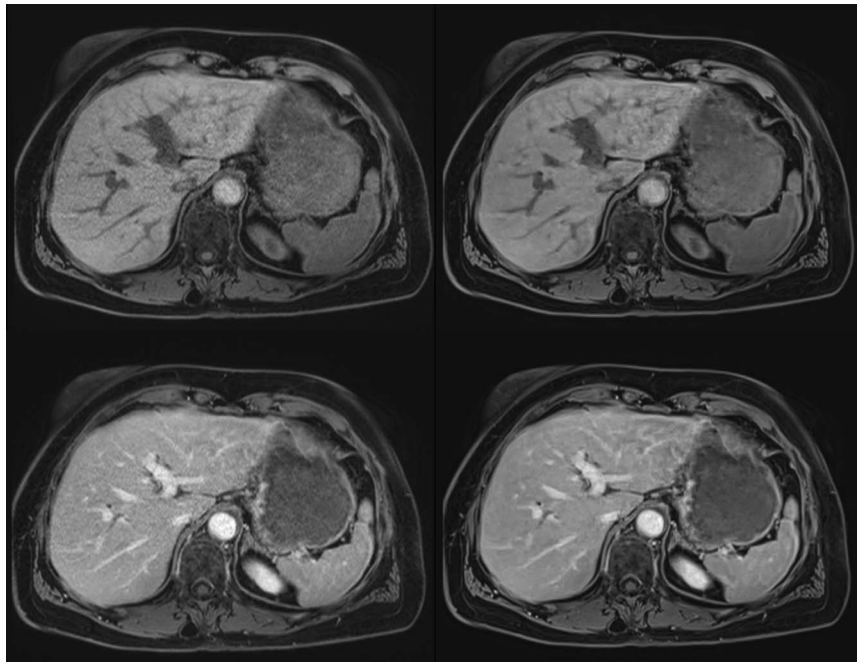

FIGURE 4. Image shows another example of standard VIBE reconstructions ($VIBE_S$; left hand side) and datasets with iterative denoising ($VIBE_{DE}$; right hand side) in precontrast (upper row) and postcontrast (bottom row) imaging. Image noise and sharpness was improved in $VIBE_{DE}$.

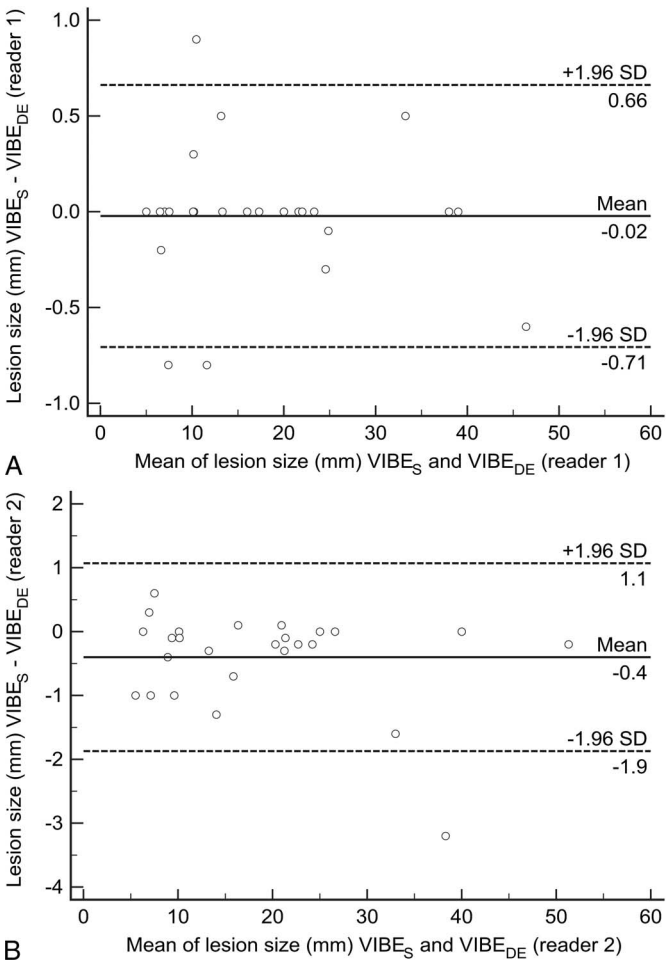

FIGURE 5. Images show Bland-Altman analysis for lesion size (millimeter) in VIBE$_S$ and VIBE$_{DE}$ for reader 1 (A) and reader 2 (B). There was no significant difference between VIBE$_S$ and VIBE$_{DE}$ in reader 1. However, lesion size in reader 2 was significantly different between VIBE$_S$ and VIBE$_{DE}$ with a systematic overestimation of 0.4 mm in VIBE$_{DE}$ ($P = 0.010$).

relatively high factors due to otherwise compromised image quality. The novel iterative denoising and image enhancement reconstruction approach presented in this study showed a significant improvement of noise levels and image quality in our patient cohort compared with VIBE$_S$. Furthermore, SNR maps in Figures 1 and 3 show an increase in SNR and also a reduced and more homogeneous distribution of noise compared with the noise band that is an issue in some cases. It becomes evident in the aforementioned examples that noise levels and SNR are especially improved in the precontrast dataset, probably due to the lack of signal in the VIBE$_S$. Furthermore, Figure 2 shows that noise artifacts caused by parallel imaging can be slightly improved using VIBE$_{DE}$. Especially the delineation of the major vessels located centrally within the body was improved demonstrating the more homogeneous noise distribution within the images. However, despite increased sharpness of structures, in most studies, there was no significant impact of the denoising and image enhancement procedure on the extent of artifacts, especially regarding motion of the intestine for example (Fig. 2).

Another advantage of this presented approach consists of its simple usability. Implementation in current scanner architecture is feasible without altering the already existing and established workflow. Neither implementation of new sequences nor special instruction for technicians is necessary. In addition, examination times can be kept to a minimum by omitting free-breathing acquisitions in uncooperative patient cohorts. Even further reduction of TA might be possible, for example, via increase of bandwidth, due to the increase of signal via the novel reconstruction algorithm. Therefore, high-quality and radiation-free imaging could be offered to a larger patient cohort.

One limitation of this study is its focus on precontrast and postcontrast abdominal MRI without analysis of dynamic contrast-enhanced (DCE) sequences. However, one of the main goals of this study was to investigate the feasibility of this iterative denoising technique in precontrast and postcontrast imaging. Consequently, DCE imaging was also no inclusion criterion for our study. As DCE imaging is often very challenging and sensitive to motion, enhancement of accelerated TA acquisitions would be of greatest interest in this field. Therefore, further studies will be necessary to investigate this area properly. In addition, other body areas should be taken into consideration to improve medical care. Another limitation that deserves consideration is the lack of quantitative SNR comparisons, which will require additional software development. However, we provided exemplarily SNR maps for precontrast and postcontrast datasets.

In conclusion, improvement of abdominal T1-weighted VIBE precontrast and postcontrast image quality, noise levels, and diagnostic confidence is possible using a novel iterative denoising and image enhancement technique. Further reduction of TA might be possible without loss of image quality.

REFERENCES

1. Keogan MT, Edelman RR. Technologic advances in abdominal MR imaging. *Radiology*. 2001;220:310–320.
2. Low RN. Abdominal MRI advances in the detection of liver tumours and characterisation. *Lancet Oncol*. 2007;8:525–535.
3. Weiss J, Martirosian P, Wolf S, et al. Fast abdominal contrast-enhanced imaging with high parallel-imaging factors using a 60-channel receiver coil setup: comparison with the standard coil setup. *Invest Radiol*. 2018;53:602–608.
4. Young WF Jr. Clinical practice. The incidentally discovered adrenal mass. *N Engl J Med*. 2007;356:601–610.
5. Ramamurthy NK, Moosavi B, McInnes MD, et al. Multiparametric MRI of solid renal masses: pearls and pitfalls. *Clin Radiol*. 2015;70:304–316.
6. Park HS, Lee JM, Choi HK, et al. Preoperative evaluation of pancreatic cancer: comparison of gadolinium-enhanced dynamic MRI with MR cholangiopancreatography versus MDCT. *J Magn Reson Imaging*. 2009;30:586–595.
7. Donato H, Franca M, Candelaria I, et al. Liver MRI: from basic protocol to advanced techniques. *Eur J Radiol*. 2017;93:30–39.
8. Budjan J, Schoenberg SO, Riffel P. Fast abdominal magnetic resonance imaging. *Rofo*. 2016;188:551–558.
9. Hargreaves BA. Rapid gradient-echo imaging. *J Magn Reson Imaging*. 2012; 36:1300–1313.
10. Markl M, Leupold J. Gradient echo imaging. *J Magn Reson Imaging*. 2012; 35:1274–1289.
11. Bitar R, Leung G, Perng R, et al. MR pulse sequences: what every radiologist wants to know but is afraid to ask. *Radiographics*. 2006;26:513–537.
12. Denolin V, Azizieh C, Metens T. New insights into the mechanisms of signal formation in RF-spoiled gradient echo sequences. *Magn Reson Med*. 2005; 54:937–954.
13. Haacke EM, Tkach JA, Parrish TB. Reduction of T2* dephasing in gradient field-echo imaging. *Radiology*. 1989;170:457–462.
14. Ludeke KM, Roschmann P, Tischler R. Susceptibility artefacts in NMR imaging. *Magn Reson Imaging*. 1985;3:329–343.
15. Elsayes KM, Narra VR, Yin Y, et al. Focal hepatic lesions: diagnostic value of enhancement pattern approach with contrast-enhanced 3D gradient-echo MR imaging. *Radiographics*. 2005;25:1299–1320.
16. Chandarana H, Block TK, Rosenkrantz AB, et al. Free-breathing radial 3D fat-suppressed T1-weighted gradient echo sequence: a viable alternative for contrast-enhanced liver imaging in patients unable to suspend respiration. *Invest Radiol*. 2011;46:648–653.
17. Rofsky NM, Lee VS, Laub G, et al. Abdominal MR imaging with a volumetric interpolated breath-hold examination. *Radiology*. 1999;212:876–884.
18. Chandarana H, Feng L, Block TK, et al. Free-breathing contrast-enhanced multiphase MRI of the liver using a combination of compressed sensing, parallel imaging, and golden-angle radial sampling. *Invest Radiol*. 2013;48:10–16.

19. Weiss J, Notohamiprodjo M, Taron J, et al. Continuous hepatic arterial multiphase magnetic resonance imaging during free-breathing. *Invest Radiol*. 2018;53:596–601.
20. Yang RK, Roth CG, Ward RJ, et al. Optimizing abdominal MR imaging: approaches to common problems. *Radiographics*. 2010;30:185–199.
21. Wang Y. Description of parallel imaging in MRI using multiple coils. *Magn Reson Med*. 2000;44:495–499.
22. Kang HJ, Lee JM, Ahn SJ, et al. Clinical feasibility of gadoxetic acid–enhanced isotropic high-resolution 3-dimensional magnetic resonance cholangiography using an iterative denoising algorithm for evaluation of the biliary anatomy of living liver donors. *Invest Radiol*. 2019;54:103–109.
23. Kannengiesser S, Maihle B, Nadar M, et al. Universal iterative denoising of complex-valued volumetric MR image data using supplementary information. *Proc ISMRM*. 2016;24:1779.
24. Blu T, Luisier F. The SURE-LET approach to image denoising. *IEEE Trans Image Process*. 2007;16:2778–2786.
25. Feng L, Grimm R, Block KT, et al. Golden-angle radial sparse parallel MRI: combination of compressed sensing, parallel imaging, and golden-angle radial sampling for fast and flexible dynamic volumetric MRI. *Magn Reson Med*. 2014;72:707–717.
26. Weiss J, Notohamiprodjo M, Martirosian P, et al. Self-gated 4D-MRI of the liver: initial clinical results of continuous multiphase imaging of hepatic enhancement. *J Magn Reson Imaging*. 2018;47:459–467.